

Corrosion impact analysis: a numerical model for reinforced concrete structures using the Finite Element Method based on Position

Chiara P. Teodoro¹, Rogério Carrazedo¹, Rodrigo S. de Melo¹

¹*Dept. of Structural Engineering, São Carlos School of Engineering/ University of São Paulo
Av. Trabalhador São Carlense 400, 13566-590, São Carlos/SP, Brazil
chiarapteodoro@usp.br, rogcarrazedo@sc.usp.br, rodrigomelo@usp.br*

Abstract. Reinforced concrete (RC) structures face environmental challenges like carbonation and chloride ingress, leading to decreased stiffness, serviceability, and security. A key issue is accurately simulating structural responses to environmental effects and their impacts. This article addresses this by proposing a numerical model using the Finite Element Method based Positions (FEMP), employing frame elements to forecast post-corrosion structural behavior. Subsequently, a probabilistic study is conducted using Monte Carlo simulations to predict failure probabilities. The study reveals corrosion's significant impact on structural stiffness and a high probability of failure after 50 years, specifically, over 75 years, using 5 mm diameter results in a failure probability 187% higher than using 10 mm diameter.

Keywords: Carbonation, Climate change, Concrete structures, Nonlinear finite element analysis, Monte Carlo simulation

1 Introduction

Reinforced concrete (RC) structures, widely used for their mechanical properties, durability and low maintenance, are susceptible to aging and deterioration from environmental conditions and excessive loads. Corrosion, induced by chlorides and carbon dioxide [1, 2], significantly diminishes the mechanical properties of concrete and steel during the propagation phase.

Environmental factors play a crucial role in the corrosion of RC structures. Variables such as temperature, humidity, the concentration of carbon dioxide (CO₂) and chlorides (Cl⁻), the duration of rain or snow periods, as well as the water-to-cement ratio (W/C), concrete compressive stress, and cover depth, significantly influence the corrosion process [2, 3]. Corrosion compromises the safety and comfort of occupants, potentially leading to excessive displacement, strains, or even structural collapse, and also carries significant economic implications (USD 2.5 trillion globally [4]).

These consequences are expected to escalate in the future due to the worsening effects of climate change on corrosion processes over time [5, 6]. Rising temperatures, increased CO₂ concentrations, and higher humidity levels from more frequent precipitation collectively elevate the risk of corrosion. Studies by Stewart, Wang, and Nguyen [5, 7] have shown that in Australia, the risks of carbonation and chloride-induced damage could significantly increase by 2100, recommending increased design cover to mitigate these effects. In China, Peng and Stewart [8] predict a 45% increase in carbonation depth by 2100, with additional damage ranging from 7-20% in certain climates. These studies collectively highlight the significant impact of climate change on structural durability and performance and the urgent need to simulate corrosion on our RC structures. Within this domain, both experimental and numerical works have examined the effects of corrosion on RC structures.

Researchers have focused on various aspects, including crack formation due to the expansion of corrosion products, reduction in rebar cross-section area, and loss of bond between concrete and steel. The reduction in rebar area directly impacts the stiffness and strength of structures [9, 10]. Furthermore, rebar diameter plays a crucial role in corrosion, as El Hassan et al. [11] demonstrated that structures using smaller diameter rebars had higher failure probabilities compared to those with larger diameters. Several notable studies have explored the numerical analysis of RC structures with reduced rebar diameters as a consequence of corrosion, offering valuable insights into the effects of decreasing rebar diameters on structural response [12–14].

RC structures are classified as composite materials, comprising a macroscopic combination of two materials to form a single functional material. Composite materials can be categorized as fibrous, laminated, particulate

composite materials, or a combination thereof [15]. In this study, RC is treated as a laminate composite material, allowing for the separate treatment of the physical nonlinearity of each material at each node [16].

This work adopted the approach of Teodoro and Carrazedo [16], where the numerical model utilized is the Finite Element Method based on Position (FEMP), naturally accounting for geometric nonlinearity through Green strains. FEMP employs current nodal positions as primary variables, ensuring a geometrically exact nonlinear description. Previous works [17–19] have provided comprehensive overviews of trusses, plates, shells, and solids formulations utilizing FEMP. Given the distinctive challenges posed by damaged corroded RC structures, where geometric nonlinearity becomes more pronounced, FEMP emerges as a suitable option.

This paper explores the utilization of FEMP using laminated frame elements, incorporating physical nonlinearity into the numerical model through the Mazars damage model [20]. It analyzes the corrosion process and formulates the modeling of rebar area reduction under corrosion. Additionally, the adopted numerical model is described, followed by the presentation and comparison of the obtained results with those reported in the literature for validation and evaluation purposes. Furthermore, a program employing FEMP to determine the probability of failure with respect to the Serviceability Limit State (SLS) of excessive displacement, according to NBR 6118 [21], was conducted using Monte Carlo simulation. This program integrates laminated frame elements combined with the Mazars damage model [20] for concrete to simulate the behavior of a beam under various configurations during the propagation stage of corrosion. The discussion presented herein encompasses aspects of nonlinear numerical analysis, the consequences of carbonation on the behavior of the structure, and reliability analyses.

2 Finite element based on positions using frame elements

The FEMP deviates from conventional FEM by utilizing positions rather than displacements as nodal variables. This methodology has been extensively applied in various works [17, 19, 22], each serving distinct objectives. FEMP employs a total Lagrangian description, seeking the gradient of the change of configuration function, which describes the transition from an initial fixed configuration to the current equilibrium configuration. Nodal positions are determined by the principle of minimum total potential energy, giving rise to nonlinear equations solvable via the iterative Newton-Raphson method.

The gradient of the configuration change function is expressed through a composition of mappings from nondimensional space to current configuration and vice versa, defined by parametric nondimensional coordinates based on initial and current body positions. The numerical frame model employs four degrees of freedom (DOF) for each node, representing positions in the 2D Cartesian coordinate system, rotation, and thickness variation. Green-Lagrange strain and Saint-Venant-Kirchhoff constitutive model are employed, naturally considering large displacements.

In simulating RC structures, the homogeneous frame element can consider equivalent area and inertia, or employ composite material theories such as fiber-reinforced composites. Laminates are approached through Equivalent Single Layer (ESL) theory or discrete-layer theories, with the First-Order Shear Deformation Theory (FSDT) being a computationally efficient choice for analyzing global structural behavior. This study enhances FSDT by incorporating a specific kinematic approach to introduce the zig-zag effect. Material nonlinearity is represented through the Mazars damage model coupled with perfect plasticity of steel rebar, as detailed in Teodoro and Carrazedo [16].

The gradient of the configuration change function is expressed through a composition of the gradient of the mapping from the nondimensional space to the current configuration, and the gradient of the inverse of the mapping from the initial configuration to the nondimensional space. These mappings are defined by parametric nondimensional coordinates, which are a function of the initial and current positions of the body.

3 Corrosion due to carbonation

The corrosion of steel rebars entails an electrochemical process involving the anodic dissolution of iron and the cathodic reduction of oxygen, with concrete pores acting as the electrolyte. Aggressive agents such as carbon dioxide (CO_2) and chloride ions (Cl^-) significantly influence this process [2]. Concrete's alkaline nature normally passivates embedded rebars; however, this protection can be compromised by Cl^- ions or the reduction in concrete alkalinity due to carbonation [23].

Different types of corrosion exhibit distinct characteristics, primarily in terms of morphology. Carbonation typically leads to a relatively uniform corrosion front, affecting the entire rebars' extent. Conversely, chloride-induced corrosion tends to be localized, manifesting as pits [11]. Carbonation-induced corrosion occurs when CO_2 , which penetrates the concrete mainly from absorption and diffusion, reacts with cement hydration products like calcium hydroxide ($\text{Ca}(\text{OH})_2$), forming calcium carbonate (CaCO_3) and water. This reaction decreases the

alkalinity in the pores around the rebar [24]. Under favorable temperatures, these reactions can disrupt the chemical stability of the passive layer, leading to rebar depassivation [2]. This type of corrosion is prevalent in industrial and urban areas with high CO₂ concentration.

Through the corrosion process, we can discern two distinct stages: initiation and propagation [25]. The initiation phase for carbonation is closely tied to the carbonation depth, which signifies the depth at which aggressive agents permeate the concrete. Once these agents reach the rebar, the initiation stage concludes. This phase involves processes such as CO₂ ingress, decalcification of the concrete, pH reduction in the porous zone, and depassivation [2].

The propagation stage commences upon depassivation and persists until structural collapse. Throughout this phase, detrimental effects occur in both the concrete and steel components. This includes the generation of corrosion products, which have larger volumes than the original steel, leading to the formation of cracks in the concrete. Additionally, the cross-sectional area of the rebar diminishes, the bond strength between the concrete and steel deteriorates, and the stress at which the rebars yield decreases. In the absence of maintenance, the structure experiences stiffness loss and gradually undergoes deformation until collapse [2, 10, 23]. This study solely considers the consequences of corrosion as the reduction in rebar cross-section. The decrease in steel yield and ultimate stress are directly linked to the corresponding loss in rebar mass, as demonstrated by Apostolopoulos and Papadakis [1] through their experimental investigations.

Reduction of rebar cross section area After depassivation, corrosion induces both chemical and mechanical degradation of the rebars, resulting in a reduction of their cross-sectional area. The rate of this degradation is quantified by the corrosion rate (i_{corr}), typically expressed in electrochemical units such as $\mu\text{A}/\text{cm}^2$ or mA/m^2 . Various empirical models estimate i_{corr} , which can be either constant or time-dependent. Numerous studies review these models, including those by Otieno et al. [26], and Sun et al. [27].

Val and Melchers [28] and Andrade and Alonso [29] utilized Faraday's law and the density of the material to correlate i_{corr} (in $\mu\text{A}/\text{cm}^2$) with the loss of steel V_{corr} (mm/yr): $V_{corr}(\text{mm}/\text{yr}) = 0.0116i_{corr}(\mu\text{A}/\text{cm}^2)$ for uniform corrosion. From this relationship, many researchers, such as Andrade et al. [30], Val et al. [12, 28], and Bastidas-Arteaga et al. [31], have used eq. (1) to determine the loss of cross-section for uniform corrosion:

$$\phi(T) = \phi_0 - 0.0232 \int_{T_i}^T i_{corr}(t) dt \quad (1)$$

where $\phi(T)$ is the diameter of the rebar under corrosion from time T_i to T (in years) and ϕ_0 is the initial diameter at time T_i , both in mm.

4 Reliability Analysis

Given the uncertainties associated with climate change, loading intensity, types of concrete, and design parameters, a reliability assessment is essential. Reliability refers to the probability that a system does not fail within a specified design life and under defined operating conditions, as the complement of the failure probability [32]. In this context, "failure" encompasses any undesirable behavior of the structure, not just system collapse. The primary challenge in structural reliability is incorporating uncertainties into a realistic model. Parameters critical to the model are treated as random variables rather than deterministic values due to the statistical nature of the data.

To predict the structural lifetime of structures under corrosion, several researchers have utilized Monte Carlo simulation [3, 7, 33]. This method involves testing a numerical model multiple times to generate a set of solutions that mimic laboratory experiments. The process includes generating random samples, evaluating failure occurrences, and estimating both failure probability and variance [32]. These simulations effectively account for the nonlinear response of structures subjected to corrosion, making them suitable for analyzing both serviceability and ultimate limit states.

Probability of failure According to NBR 6118 [21], a concrete structure must be evaluated for Serviceability Limit States (SLS), including excessive displacement, crack formation, crack width, excessive vibration, among others. These limits are related to the structure's durability, user comfort, appearance, and proper utilization of the structures.

In this study, only the SLS concerning displacement within the sensory acceptability (user comfort) is evaluated, meaning that the permissible deflection for the structure (RC beam) is $\frac{\ell}{250}$, where ℓ is the span length. It is understood that reaching this limit may or may not imply that the structure has reached other SLS, but only excessive displacement was considered herein.

Thus, the limit state equation for failure in the propagation stage due to the excessive deflection is defined in section 4, where $y(t, \text{midspan})$ is the midspan deflection at time step t :

$$g_3(\mathbf{x}) = \frac{\ell}{250} - y(t, \text{midspan}) \quad (2)$$

5 Results and discussion

5.1 Validation of a corroded beam

The chosen beam Fig. 1 provides data for simulating concrete structures under corrosion and bending, using experimental data from Castel *et al.* [34] and numerical data from Biondini and Vergani [13]. Although focused on chloride-induced corrosion, a uniform corrosion rate was applied expecting similar outcomes due to the uniformity of corrosion at the midspan.

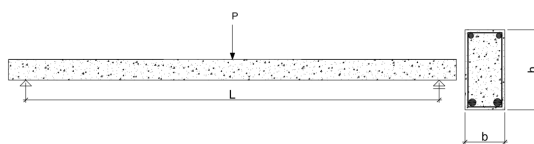


Figure 1. Configuration of beams subjected to natural corrosion experimental tests.

In their experimental study, Castel *et al.* [34] exposed a RC beam to salt spray and subjected it to a three-point bending test. The beam dimensions were $L = 300$ cm, $b = 15$ cm, $h = 28$ cm, with a concrete cover of 1 cm. The beam was reinforced with two tensile bars of $\phi = 12$ mm and two compressive bars of $\phi = 6$ mm. After 14 years, the non-corroded beam (BIT) and the corroded beam (B1CL) showed average compression stresses of 65.3 MPa and 63.4 MPa, respectively, with elastic moduli of 36.3 GPa and 35.0 GPa. The tensile bars experienced an average maximum reduction in the steel cross-section of about 20% in the central part. Biondini and Vergani [13] performed a nonlinear numerical analysis assuming a steel cross-section loss of 22%.

In this study, a uniform corrosion of 20% was applied using a mesh of 60 elements and 30 load steps of 2 kN. The tolerance used was 10^{-7} , and the adopted Mazars parameters were: $A_T = 0.82$, $A_C = 1.5$, $B_T = 18000$, and $B_C = 1620$. Fig. 2 compares the numerical (Num.) and experimental (Exp.) results, focusing on the force-displacement graph at midspan. Initially, the experimental model exhibits elastic behavior up to approximately 12 kN, after which the concrete undergoes damage, leading to a minor decay. When the steel yields (about 44 kN in BIT and 38 kN in B1CL), the concrete is nearly fully damaged. As plastification continues, the structure achieves ultimate strength. The numerical results closely mirror the experimental findings, showing similar stages of behavior with comparable load and displacement values.

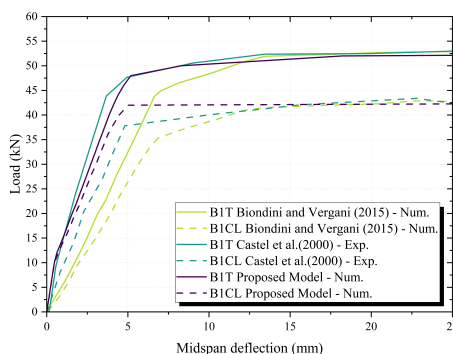


Figure 2. Comparison between experimental and numerical results for beams under natural corrosion.

While the overall behavior of the structure in both the numerical and experimental models was similar, differences were observed in the curvature of the graph during the steel plastification stage. These variations are

attributed to different modeling approaches for the steel. This study employed perfect plasticity, resulting in a steeper curve.

5.2 Probability of failure of a 75 years old beam

The choice of variables depends on the specific case under study. In this investigation, the failure probability of the beam studied by Álvares [30], shown in Fig. 3, was calculated considering the variables: corrosion rate ($\mu\text{A}/\text{cm}^2$) follows a lognormal distribution with a mean value of 0.5 and a coefficient of variation of 1.00, as reported by Peng and Stewart [35]; the external load (kN) is modeled with a Gumbel distribution, having a mean value of 36.0 and a coefficient of variation of 0.10; the concrete cover (cm) is normally distributed with a mean value of 3.0 and a coefficient of variation of 0.12, referenced from Félix and Carracedo [36]. Concrete covers were selected to meet the requirements of NBR 6118 [21]. Calculations were performed at six-time intervals: 0, 15, 30, 45, 60, and 75 years, spanning the propagation period and assuming depassivation had already occurred. A time span exceeding 50 years was included as the structure's failure time is expected to be longer. Details of the numerical model are provided by Teodoro and Carracedo [16].

One key characteristic of uniform corrosion, as described in eq. (1), is that smaller rebar cross-sections are more prone to damage because $\Delta\phi$ depends on i_{corr} , T , and V_{corr} , which are independent of the rebar diameter [37]. Building on this, the failure probability was calculated for the original experiment, which used three bars with a diameter of 10 mm, and alternatively, for 12 bars with a diameter of 5 mm, resulting in the same reinforcement area. The probability of failure over time is presented in Fig. 4. A total of 10^4 samples were used for the beam with 5 mm bars and 4×10^4 samples for the beam with 10 mm bars to ensure a 95% confidence interval.

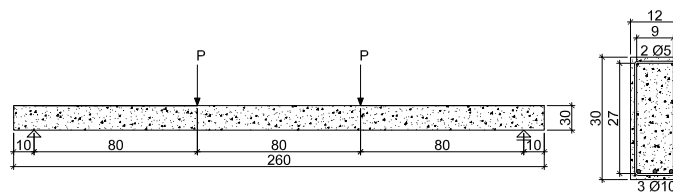


Figure 3. Experimental test configuration of a RC beam by Álvares [30]. Dimensions in cm and the stirrups were not considered in the calculation

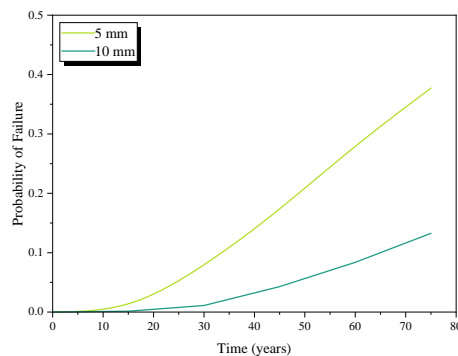


Figure 4. Probability of failure over the years for the beam of the work of Álvares[30].

The results on the probability of flexural failure yield several important conclusions:

- **Reinforcement Diameter:** The choice of reinforcement diameter is crucial, especially in environments with high aggressiveness, such as industrial areas with elevated CO_2 levels.
- **Failure Probability:** As shown in Fig. 4, the probability of failure aligns with findings by El Hassan et al. [11], who concluded that the probability of failure for a RC bridge beam in its ultimate flexural state is higher for structures using more small-diameter bars compared to fewer large-diameter bars. The failure probability is three times higher when using nine bars of 20 mm compared to six bars of 25 mm.
- **Corrosion Impact:** Smaller diameter bars degrade more significantly due to corrosion, potentially altering the failure mode of the structure. As corrosion progresses, stirrups and compression reinforcement may

lose their structural function, while larger diameter flexural reinforcement can continue to function at an acceptable level.

Failure due to excessive displacement is less likely with larger diameters. Over 75 years, using 5 mm diameter results in a failure probability 187% higher than 10 mm. This study did not consider variables such as bond loss between steel and concrete, reduced concrete strength from cracking, and decreased steel yield strength.

6 Conclusions

In this study, we provided a condensed analysis to anticipate the impacts of corrosion on structures in the propagation stage. For the analysis of structural failure in the excessive displacement (SLS), the Finite Element Method based on Positions, employing laminated frame elements, was utilized to calculate structural response under corrosion and external loads.

The comparison with experimental tests highlights the effectiveness of this approach in simulating the behavior of a corroding structure. By predicting the reduction in the steel's cross-sectional area, the numerical program can forecast the structure's long-term behavior. This analysis has revealed an increased vulnerability to corrosion when smaller rebar diameters are used. The numerical model shows that using 5 mm diameter increases failure probability by 311% within 45 years compared to 10 mm, using equivalent reinforcement areas. A failure probability above 10% occurs in 33 years for 5 mm and 65 years for 10 mm diameters.

A significant concern arises as we project 50 years ahead. This concern is heightened in Brazil, not only due to the worrisome results of the analysis considering only the increase in CO₂ concentration, but also due to the predicted rise in temperature and humidity in certain regions, which is expected to further exacerbate the situation. Compounding this, many constructions in Brazil do not adhere to the prescribed standards for concrete cover, bringing up a concerning situation for the future. Addressing this multifaceted concern will be a primary focus of our future research, aiming to develop a more comprehensive understanding of the climate-induced effects on structural durability and performance.

Acknowledgements. This work is supported by FAPESP (Fundação de Amparo à Pesquisa do Estado de São Paulo), grant 2023/13093-9 for Chiara P. Teodoro.

Authorship statement. The authors hereby confirm that they are the sole liable persons responsible for the authorship of this work, and that all material that has been herein included as part of the present paper is either the property (and authorship) of the authors, or has the permission of the owners to be included here.

References

- [1] C. A. Apostolopoulos and V. Papadakis. Consequences of steel corrosion on the ductility properties of reinforcement bar. *Construction and Building Materials*, vol. 22, pp. 2316–2324, 2008.
- [2] R. Rodrigues, S. Gaboreau, J. Gance, I. Ignatiadis, and S. Betelu. Reinforced concrete structures: A review of corrosion mechanisms and advances in electrical methods for corrosion monitoring. *Construction and Building Materials*, vol. 269, pp. 121240, 2021.
- [3] E. Bastidas-Arteaga, A. Chateauneuf, M. Sánchez-Silva, P. Bressolette, and F. Schoefs. Influence of weather and global warming in chloride ingress into concrete: A stochastic approach. *Structural Safety*, vol. 32, pp. 238–249, 2010a.
- [4] G. Koch. Cost of corrosion. In A. El-Sherik, ed, *Trends in Oil and Gas Corrosion Research and Technologies*, pp. 3–30. Woodhead Publishing, Boston, 2017.
- [5] M. G. Stewart, X. Wang, and M. N. Nguyen. Climate change impact and risks of concrete infrastructure deterioration. *Engineering Structures*, vol. 33, pp. 1326–1337, 2011.
- [6] E. Bastidas-Arteaga. Reliability of reinforced concrete structures subjected to corrosion-fatigue and climate change. *Engineering Structures*, vol. 51, 2013.
- [7] M. G. Stewart, X. Wang, and M. N. Nguyen. Climate change adaptation for corrosion control of concrete infrastructure. *Structural Safety*, vol. 35, pp. 29–39, 2012.
- [8] L. Peng and M. G. Stewart. Climate change and corrosion damage risks for reinforced concrete infrastructure in China. *Structure and Infrastructure Engineering*, vol. 12, n. 4, pp. 499–516, 2016.
- [9] G. J. Cabrera. Deterioration of concrete due to reinforcement steel corrosion. *Cement and Concrete Composites*, vol. 18, pp. 47–59, 1996.
- [10] W. Zhu and R. François. Corrosion of the reinforcement and its influence on the residual structural performance of a 26-year-old corroded rc beam. *Construction and Building Materials*, vol. 51, pp. 461–472, 2014.

- [11] J. El Hassan, P. Bressolette, A. Chateauneuf, and K. El Tawil. Reliability-based assessment of the effect of climatic conditions on the corrosion of rc structures subject to chloride ingress. *Engineering Structures*, vol. 32, pp. 3279–3287, 2010.
- [12] D. V. Val, M. G. Stewart, and R. E. Melchers. Effect of reinforcement corrosion on reliability of highway bridges. *Engineering Structures*, vol. 20, pp. 1010–1019, 1998.
- [13] F. Biondini and M. Vergani. Deteriorating beam finite element for nonlinear analysis of concrete structures under corrosion. *Structure and Infrastructure Engineering*, vol. 11, pp. 519–532, 2015.
- [14] D. V. Val and L. Chernin. Serviceability reliability of reinforced concrete beams with corroded reinforcement. *Journal of Structural Engineering*, vol. 135, pp. 896–905, 2009.
- [15] R. M. Jones. *Mechanics of composite materials*. Taylor & Francis, Philadelphia, 1999.
- [16] C. P. Teodoro and R. Carrazedo. Nonlinear numerical analysis of corroded reinforced concrete structures using laminated frame elements. *Materials and Structures*, vol. 57, pp. 109, 2024.
- [17] R. Carrazedo and H. B. Coda. Alternative positional fem applied to thermomechanical impact of truss structures. *Finite Elements in Analysis and Design*, vol. 46, pp. 1008–1016, 2010.
- [18] H. B. Coda and R. R. Paccola. Improved finite element for 3d laminate frame analysis including warping for any cross-section. *Applied Mathematical Modelling*, vol. 34, pp. 1107–1137, 2010.
- [19] H. B. Coda, R. R. Paccola, and R. Carrazedo. Zig-zag effect without degrees of freedom in linear and non linear analysis of laminated plates and shells. *Composite Structures*, vol. 161, pp. 32–50, 2017.
- [20] J. Mazars and G. Pijaudier-Cabot. Continuum damage theory—application to concrete. *Journal of Engineering Mechanics*, vol. 115, pp. 345–365, 1989.
- [21] ABNT:NBR6118. *Design of concrete structures: procedure*. Associação Brasileira de Normas Técnicas, Rio de Janeiro, Brazil, 2023.
- [22] R. Carrazedo and H. B. Coda. Triangular based prismatic finite element for the analysis of orthotropic laminated beams, plates and shells. *Composite Structures*, vol. 168, pp. 234–246, 2017.
- [23] V. G. Papadakis, C. G. Vayenas, and M. N. Fardis. A reaction engineering approach to the problem of concrete carbonation. *AIChE Journal*, vol. 35, pp. 1639–1650, 1989.
- [24] L. Basheer, J. Kropp, and D. J. Cleland. Assessment of the durability of concrete from its permeation properties: a review. *Construction and Building Materials*, vol. 15, pp. 93–103, 2001.
- [25] K. Tuutti. *Corrosion of steel in concrete*. Swedish Cement and Concrete Research Institute, Stockholm, 1982.
- [26] M. B. Otieno, H. D. Beushausen, and M. G. Alexander. Modelling corrosion propagation in reinforced concrete structures – a critical review. *Cement and Concrete Composites*, vol. 33, pp. 240–245, 2011.
- [27] B. Sun, R. C. Xiao, W. D. Ruan, and P. B. Wang. Corrosion-induced cracking fragility of rc bridge with improved concrete carbonation and steel reinforcement corrosion models. *Engineering Structures*, vol. 208, pp. 110313, 2020.
- [28] D. V. Val and R. E. Melchers. Reliability of deteriorating rc slab bridges. *Journal of Structural Engineering*, vol. 123, pp. 1638–1644, 1997.
- [29] C. Andrades and C. Alonso. Test methods for on-site corrosion rate measurement of steel reinforcement in concrete by means of the polarization resistance method. *Materials and Structures*, vol. 37, pp. 623–643, 2004.
- [30] M. S. Alvares. Estudo de um modelo de dano para o concreto: formulação, identificação paramétrica e aplicação com emprego do método dos elementos finitos, 1993.
- [31] E. Bastidas-Arteaga, F. Schoefs, M. G. Stewart, and X. Wang. Influence of global warming on durability of corroding rc structures: A probabilistic approach. *Structural Safety*, vol. 32, pp. 238–249, 2010b.
- [32] R. E. Melchers and A. T. Beck. *Structural reliability analysis and prediction*. John Wiley & sons, UK, 2018.
- [33] U. J. Na, S.-J. Kwon, S. R. Chaudhuri, and M. Shinozuka. Stochastic model for service life prediction of RC structures exposed to carbonation using random field simulation. *KSCCE Journal of Civil Engineering*, vol. 16, n. 1, pp. 133–143, 2012.
- [34] A. Castel, R. Francois, and G. Arliguie. Mechanical behaviour of corroded reinforced concrete beams—part I: Experimental study of corroded beams. *Materials and Structures*, vol. 33, pp. 539–544, 2000.
- [35] L. Peng and M. G. Stewart. Carbonation-induced corrosion damage and structural safety for concrete structures under enhanced greenhouse conditions. Technical report, Centre for Infrastructure Performance and Reliability - University of Newcastle, 2008.
- [36] E. F. Felix and R. Carrazedo. Análise probabilística da vida útil de lajes de concreto armado sujeitas à corrosão por carbonatação via simulação de monte carlo. *Matéria (Rio de Janeiro)*, vol. 26, pp. e13043, 2021.
- [37] M. B. Otieno, H. D. Beushausen, and M. G. Alexander. Prediction of corrosion rate in reinforced concrete structures – a critical review and preliminary results. *Materials and Corrosion*, vol. 63, pp. 777–790, 2012.